ACS APPLIED MATERIALS & INTERFACES

Research Article

www.acsami.org

pH-Manipulated Underwater–Oil Adhesion Wettability Behavior on the Micro/Nanoscale Semicircular Structure and Related Thermodynamic Analysis

Lu Tie,[†] Zhiguang Guo,*[,†,‡] and Weimin Liu[†]

[†]State Key Laboratory of Solid Lubrication, Lanzhou Institute of Chemical Physics, Chinese Academy of Sciences, Lanzhou 730000, China

[‡]Hubei Collaborative Innovation Centre for Advanced Organic Chemical Materials and Ministry of Education Key Laboratory for the Green Preparation and Application of Functional Materials, Hubei University, Wuhan 430062, China

ABSTRACT: Controlling oil of wettability behavior in response to the underwater out stimulation has shown promising applications in understanding and designing novel micro- or nanofluidic devices. In this article, the pH-manipulated underwater–oil adhesion wetting phenomenon and superoleophobicity on the micro- and nanotexture copper mesh films (CMF) were investigated. It should be noted that the surface exhibits underwater superoleophobicity under different pH values of the solution; however, the underwater–oil adhesion behavior on the surface is dramatically influenced by the pH value of the solution. On the basis of the thermodynamic analysis, a plausible mechanism to explain the pH-controllable underwater–oil adhesion and superoleophobic wetting behavior observed on a micro- and nanoscale semicircular structure has been revealed. Furthermore, variation of chemistry (intrinsic oil contact angle (OCA)) of the responsive surface that due to the carboxylic acid groups is protonated or deprotonated by the acidic or basic solution on free energy (FE) with its barrier (FEB) and equilibrium oil contact angle (EOCA) with it hysteresis (OCAH) are discussed. The result shows that a critical intrinsic OCA on the micro- and nano- semicircular texture is necessary for conversion from the oil Cassie impregnating to oil Cassie wetting state. In a water/oil/solid system, the mechanism reveals that the differences between the underwater OCA and oil adhesive force of the responsive copper mesh film under different pH values of solution are ascribed to the different oil wetting state that results from combining the changing intrinsic OCA and micro-/nanosemicircular structures. These results are well in agreement with the experiment.

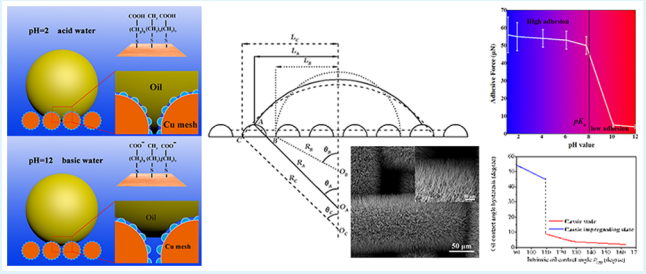

KEYWORDS: *oil adhesion, superoleophobic, free energy, equilibrium oil contact angle, Cassie impregnating*

1. INTRODUCTION

Learning from nature, for example, lotus leaves,[1] rose petals,[2] fish,[3] and water strider's legs,[4] attention has always been paid to preparing artificial interfacial materials with special wetting functions. Nowadays, many efforts have been devoted to exploring responsive surfaces with switchable adhesion in the air, under out stimulations, for example light,[5] electricity,[6] magneticity,[7] pH,[8] and thermal treatment.[9] Besides, controllable oil-adhesion on underwater superoleophobic surfaces has been demanded for solving interface science problems such as novel micropatterning and smart microfluidic gates.[10,11] Based on the surface with manipulated oil of wettability in response to the out stimulations under underwater circumstances, the pH-manipulated water permeation and water–oil separation film are examined,[12,13] which are useful in designing novel micro- and nano-devices[14] for advanced applications. Meanwhile, responsive oil adhesion is helpful with oil control and transportation under underwater circumstances. Although a lot of research has been done in this area, pH-controllable oil adhesion under underwater circumstances is still relatively rare.

There are two dominant approaches for controlling surface adhesion. One can use low free energy surface chemical composition or strengthen surface roughness.[15−21] Recently, many studies with affection for microstructures on the adhesive property have been investigated, while the affection of surface chemistry on surface adhesion is relatively rare, especially for underwater pH-controllable environments. Here, a novel method for the fabrication of controllable adhesive superoleophobic surfaces by modifying the chemical molecular response on the micro- and nano-structured copper mesh film (CMF) is proposed, and the effect of environmental pH value on the responsive adhesion behavior is investigated. Compare this work with others, the merits of this method are devoted to developing a model for the wetting behavior of the CMF. Furthermore, the model can explain the wetting mechanism of the CMF. In a water/oil/solid system, the carboxylic acid

Received: April 23, 2015
Accepted: April 28, 2015
Published: April 28, 2015

DOI: 10.1021/acsami.5b03533
ACS Appl. Mater. Interfaces 2015, 7, 10641−10649

groups are protonated or deprotonated for the acidic or basic solution, resulting in the variation with the intrinsic OCA on responsive copper mesh films, while surface chemistry (intrinsic OCA) plays an important part in determining the value of the oil contact angle (OCA) and its hysteresis (OCAH). Therefore, the oil controllable adhesion is due to the different wetting states on the responsive superoleophobic surface that results from different intrinsic OCAs under different environmental pH values.

In the theoretical aspect, nowadays, many simulations have been done to design optimal superhydrophobic and superoleophobic surfaces.[22−29] Based on these studies, we analyze the theoretical model using thermodynamics. Particularly, this model can solve the more important CAH. Recently, a thermodynamic approach was investigated.[30] Unfortunately, the flat pillar microtexture surface is investigated in this mode. In fact, the actual microtexture of superhydrophobic surfaces possesses a circular top. In this paper, based on the thermodynamic approach to analyze the FE and FEB of a metastable wetting state,[30−32] this issue both analytically and numerically is presented. A general semicircular micro- and nanotexture surface is developed to explain the mechanism of oil wetting behavior. Particularly, this semicircular microtexture is easy to fabricate in large enough quantities since semicircular microtexture has not edges nor corners. Thus, it possesses good mechanical properties. Meanwhile, the semicircular microtexture is similar to the actual microtexture structure which has been investigated in the experiment. Besides, compared with another reported paper,[30,31] this paper mainly focuses on the affection of intrinsic OCA on wetting behavior which has been experimentally emphasized. More importantly, we extend the model to solve the oil wetting behavior with an underwater environment.

2. pH-RESPONSIVE UNDWEWATER OIL-ADHESION WETTING BEHAVIOR OF MICRO- AND NANO-STRUCTURED CMF

Figure 1a exhibits the SEM image of the original copper mesh film (CMF). It is shown that the original CMF is relatively

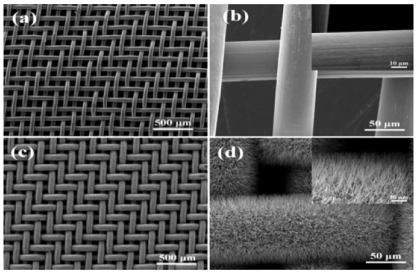

Figure 1. SEM images of the original (a, b) and $Cu(OH)_2$ coated on superoleophobic CMF (c, d). The insets in b and d show the larger view of single mesh wires.

smooth and the oil contact angles (OCA) are relatively lower and unstable. The large view of the original mesh shows that the diameter of one copper wire and the value of one square pore are about 50 μm as illustrated in Figure 1b, respectively. Furthermore, from Figure 1c and d, it can be found that the microscale and many $Cu(OH)_2$ nanoscale copper wires are grown on the copper mesh. The $Cu(OH)_2$ nanoscale copper wires exhibited uniformly, with an average nanowire diameter of 200 nm and a length of 10 000 nm. Importantly, it is noted that the high magnification of the SEM images (Figure 1d) consisted of many nanowires among them. The micro- or nanohierarchical rough structures are vital to the underwater−oil wetting behavior.

It is noted that the CMF exhibits underwater superoleophobicity under different pH value solutions, and the OCA of the mesh film with pH = 12 is about 10° bigger than that with pH = 2, as shown in Figure 2. It is clear that the

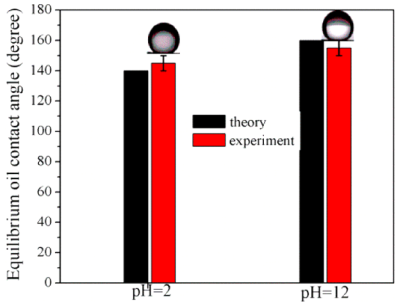

Figure 2. Underwater equilibrium oil contact angle (EOCA) of the micro- and nanoscale structured CMF to different oil droplets in acidic (pH = 2) and basic (pH = 12) solutions.

experimental results are consistent with the theory. Additionally, the underwater−oil adhesive force of the CMF under different pH values of the solution is measured by a high sensitivity microelectromechanical balance system. Then, the relationship between the adhesion force and distance was recorded as shown in Figure 3. It should be noted that the oil

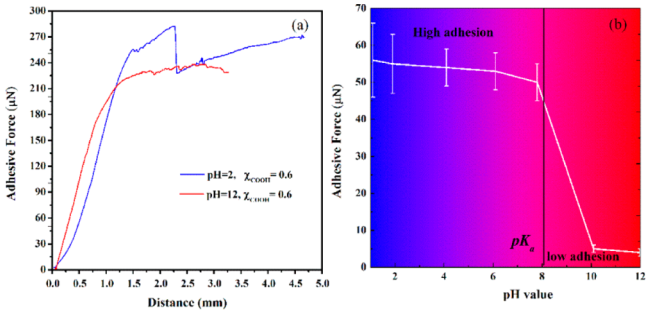

Figure 3. pH-manipulated underwater oil-adhesion wetting behavior of the micro- and nanoscale structured CMF. (a) Adhesive force versus distance curves recorded with an underwater oil droplet under different pH values. (b) Variation of underwater oil adhesive force against distance under different pH values (1,2-dichloroethane, 4 μL).

adhesion force of the micro- or nanotexture $Cu(OH)_2$ mesh films underwater is dramatically influenced by the pH value of solution. From Figure 3a, one can see that the oil adhesive force of the CMF for the pH = 2 solution with 48.0 ± 1 to 65.0 ± 1 μN is larger than that for the pH = 12 solution with 3 ± 0.2 to 5 ± 0.2 μN. The underwater oil-adhesion on the micro- or nanoscale structure $Cu(OH)_2$ mesh films increased with the pH, as shown in Figure 3b. One can clearly see that the oil adhesion dramatically decreases with increasing pH from 8.0 to 10.0. When the pH value is lower than 8.0, the CMF shows high oil adhesion, but the situation is opposite of that when the pH value is larger than 10.0. At a low pH, when the pH value is less than the pK_a value of the $HS(CH_2)_{10}COOH$, the carboxylic groups on neighboring $HS(CH_2)_{10}COOH$ are protonated by the acidic solution. The oil wetting state is the Cassie

DOI: 10.1021/acsami.5b03533
ACS Appl. Mater. Interfaces 2015, 7, 10641−10649

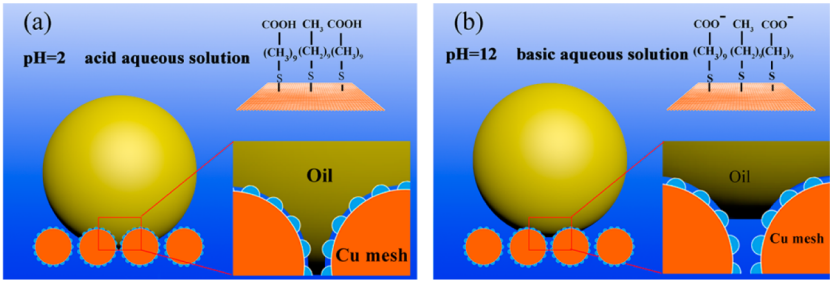

Figure 4. Under acidic solution conditions, an oil droplet can be adhesive on the surface (a). (X_{COOH} = 0.6), while under basic solution conditions, oil droplets easily roll (b). Reversible transitions between the Cassie impregnating wetting state and Cassie state wetting state can be achieved by simply changing the pH value.

impregnating wetting state. But at a higher pH, when the pH value is larger than the pK_a value of the $HS(CH_2)_{10}COOH$, the carboxylic groups are deprotonated basic solution. The wetting state stays in a typical Cassie state. The difference of the underwater OCA and oil adhesive force of the CMF under different pH values of solutions is caused by changing the wetting states, owing to the carboxylic acid groups being protonated or deprotonated by an acidic or basic solution.

3. THERMODYNAMIC INVESTIGATION

3.1. Basic Wetting Theory on the Micro- and Nanoscale Hierarchical Semicircular Structure. In this section, to investigate an oleophobic surface in water, we mainly discuss the solid/water/oil interface. Similarly, if an oil droplet is located at a smooth underwater solid surface, the underwater−oil intrinsic CA θ_{ow} is given by[33]

$$\cos\theta_{ow} = \frac{\gamma^{oa}\cos\theta_o - \gamma^{wa}\cos\theta_w}{\gamma^{ow}} \quad (1)$$

where θ_o is oil intrinsic CA in air and θ_w is water intrinsic CA in air. γ^{oa}, γ^{wa}, and γ^{ow} are the surface tensions at oil−air, water−air, and oil−water interfaces. The underwater−oil wetting state with the micro- and nanotexture CMF can be explained by the intrusion pressure (ΔP) which can be described by the following equation:[34]

$$\Delta P = -l\gamma\cos\theta/A \quad (2)$$

where γ stands for the interface tension, l stands for the length of the mesh pore, A stands for the pore cross-sectional area, and θ stands for intrinsic contact angle. According to eq 2, water (γ = 72.8 mN/m) can be trapped in the micro- and nanoscale structure of the copper mesh film, owing to $\Delta P < 0$ (water intrinsic contact angle $\theta = 70° \pm 1°$ within the acid and $\theta = 49° \pm 1°$ within the basic solution on the copper mesh). 1,2-Dichloroethane (γ = 24.15 mN/m) is considered as oil. It cannot completely wet into micro- and nanoscale structure copper mesh film caused by $\Delta P > 0$ ($\theta_{ow} = 95° \pm 2°$ within an acid solution and $\theta_{ow} = 130° \pm 2°$ within a basic solution) of the CMF in water, leading to the different amount of oil wetting in the micro- and nanostructures under different pH values of solution, which cause the different oil adhesion forces. In this article, compared to the case with the Cassie impregnating and Cassie state wetting state in a water−air−solid system,[2] the situation in a water−oil−solid system with Cassie impregnating (the microroughness is completely filled with oil, the nanoroughness is filled water) and Cassie state wetting state (the micro- and nanoroughness is filled water, while oil did not penetrate into the troughs of micro- and nanoroughness) of an underwater−oil droplet residing on the micro- and nanoscale semicircular structure are proposed as shown in Figure 4. In calculation, the micro- and nanoscale semicircular structure is a composite with the semicircular base angle (α), radius (R), and spacing (b). Subscripts 1 and 2 stand for microtexture and nanotexture.

Cassie[35] et al. developed a model to calculate the contact angle in an air−water−solid system. In an underwater three phase system, an oil droplet is located at the solid and water; the apparent contact angle (θ_{CB}) of an oil droplet can be calculated by the Cassie equation:

$$\cos\theta_{CB} = r_f f\cos\theta_{ow} + f - 1 \quad (3)$$

If an oil droplet is located at the solid and oil, the apparent contact angle (θ_W) of an oil droplet can be calculated by the Wenzel equation[36]

$$\cos\theta_w = r\cos\theta_{ow} \quad (4)$$

From the result with ref 37, it is noted that the equilibrium CA equation on the micro- and nanotexture surface is the same as the typical Wenzel or Cassie−Baxter equation; only the intrinsic CA is replaced by the equilibrium CA on a nanotexture. Thus, the contact angle (θ_{CI}) for the Cassie impregnating state on the semicircular micro- and nanotexture surface can be expressed as

$$\cos\theta_{CI} = r_1\cos\theta_1 \quad (5)$$

The contact angle (θ_C) for the Cassie wetting state on the Semicircular micro- and nanotexture surface can be given:

$$\cos\theta_C = r_{f_1} f_1\cos\theta_1 + f_1 - 1 \quad (6)$$

while the effective equilibrium contact angle of the underwater−oil droplet can be defined as

$$\theta_1 = \mathrm{Arccos}(r_{f_2} f_2\cos\theta_{ow} + f_2 - 1) \quad (7)$$

where the wet area roughness ratio r_f and the solid fraction f for the 2D model with micro- and nanotexture may be represented as $r_{f1} = \alpha_1/\sin\alpha_1, f_1 = 2R_1\sin\alpha_1/(2R_1 + b_1)$, $r_{f2} = \alpha_2/\sin\alpha_2, f_2 = 2R_2\sin\alpha_2/(2R_2 + b_2)$; a roughness factor r of micro- and nano-semicircular can be defined as $r_1 = (\pi R_1 + b_1)/(2R_1 + b_1)$, $r_2 = (\pi R_2 + b_2)/(2R_2 + b_2)$. Therefore, in this article, the Cassie impregnating and Cassie wetting state can effectively investigate the microtexture noncomposite and composite oil wetting state if only the intrinsic OCA (θ_{ow}) with the microtexture noncomposite and composite state is effectively replaced with the equilibrium OCA on a nanotexture (θ_1). For a Cassie wetting state, an oil droplet is located at the top of the semicircular microstructure with oil liquid penetrating the

DOI: 10.1021/acsami.5b03533
ACS Appl. Mater. Interfaces 2015, 7, 10641−10649

troughs among semicircular protrusions; the slope angles α_1 and α_2 stand for the amount of oil penetrating the troughs between semicircular protrusions. Thus, the effective microtexture composite state may exist if the slope angle of micro- and nanosemicircular structure is equal to the critical angle α_1, α_2[38,39]

$$\alpha_2 = \pi - \theta_{ow};\ \alpha_1 = \pi - \theta_1 \tag{8}$$

Combining eqs 7 and 8, one can find that the penetrated height for the microtexture composite state depends on the underwater−oil CA on the flat surface and the geometrical parameters of semicircular nanotexture.

3.2. Thermodynamic Investigation of the Micro- and Nanosemicircular Structure. In the article, the model with a 3D system shown in Figure 1 is simplified into a 2D system along specific planes, as shown in Figures 5 and 6. There are

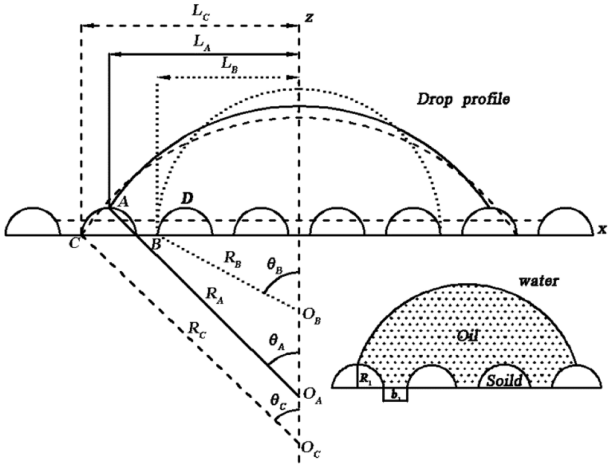

Figure 5. Illustration of variation of microtexture noncomposite wetting state for an oil droplet from state A to B (or to C) along the contact line.

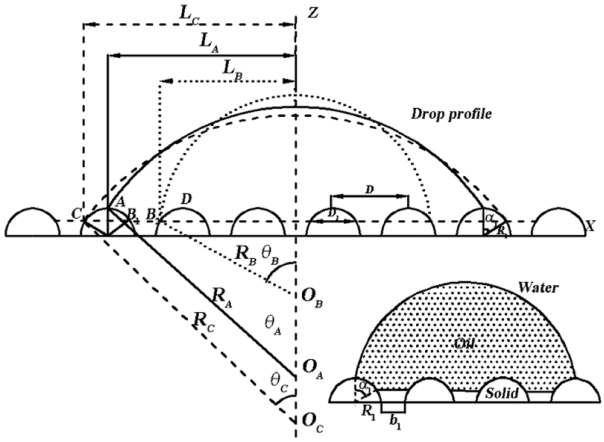

Figure 6. Illustration of variation of microtexture composite wetting state for an oil droplet from state A to B (or to C) along the contact line.

solids existing between copper wires on the specific planes. Meanwhile, the model can reflect the actually situation of a copper mesh. On the basis of thermodynamic analysis, a model of the semicircular microtextured surface with a set of geometrical parameters (see Figures 5, 6) has been developed. Some assumptions have been made as before;[30] additionally, we ignore the influence of the oil property of Lewis acid−base interactions.[40] Thus, the interface force of oil (γ^{ow}) in different pH value solutions keeps a constant value. The FE with its barrier (FEB) and CA with its hysteresis (CAH) for Cassie impregnating wetting state and Cassie state wetting state in a water/air/solid system can be numerically calculated.

3.2.1. Gibbs Free Energy (FE) and Free Energy Barrier (FEB) Analysis for the Oil Cassie Impregnating State. For a microtexture noncomposite state (see Figure 5), when the oil droplet is jumping from one semicircular protrusion to the nearby one, there exist two positions of local equilibrium extreme energy values which are vital to determine the FEB, one metastable and one unstable. The metastable position is shown schematically in Figure 5, such as the points A and D. When the oil droplet edge recedes from the point A to B, the vector which is caused by the interfacial forces balance leads to the movement of the droplet to the metastable point A. When the oil droplet edge recedes from B to D, the force vector leads to movement of the droplet edge farther from B. Thus, the position of point B is the unstable state which has the local maximum free energy when the edge of the droplet is receding from one semicircular protrusion metastable position to the nearby one. When the drop edge advances from the point A to C, the force vector also leads to movement of oil droplet approach A. Thus, the position of point A is the other unstable state which has the local maximum free energy when the edge of the droplet is advancing from one semicircular protrusion metastable position to the next.[37] The difference between local maximum and minimum FE can be used as the FEB. When the droplet recedes from point A (with a CA (θ_A) and drop size (L_A)) to B (with a CA (θ_B) and drop size (L_B)), the droplet area in the $x-z$ plane stays unchanged for the 2D model; thus, the geometrical relationship parameters (θ, R_1, b_1) can be written as

$$\theta_A \frac{{L_A}^2}{\sin^2\theta_A} - {L_A}^2 \cot\theta_A + \frac{L_A}{b_1 + 2R_1}\left[(b_1 + 2R_1)R_1 - \frac{\pi {R_1}^2}{2}\right] = \theta_B \frac{{L_B}^2}{\sin {\theta_B}^2} - {L_B}^2 \cot\theta_B - \frac{L_B}{b_1 + 2R_1}\left(\frac{\pi {R_1}^2}{2}\right) \tag{9}$$

The per unit length of free energy perpendicular in the $x-z$ plane at point A and B can be expressed as

$$F_A = \gamma^{ow} {l_A}^{ow} + \gamma^{so} {l_A}^{so} + C \tag{10}$$

$$F_B = \gamma^{ow} {l_B}^{ow} + \gamma^{sw} {l_B}^{sw} + C \tag{11}$$

where C is a constant which stands for the unchanged FE of the system. Considering the micro- and nano-semicircular structure, when eqs 1, 7, 10, and 11 are combined, the relative free energy barrier for transition from the position A to B can be expressed as

$$\frac{\Delta F_{A\to B}}{\gamma^{ow}} = \theta_B \frac{L_B}{\sin\theta_B} - \theta_A \frac{L_A}{\sin\theta_A} + \left(b_1 + \frac{\pi R_1}{2}\right)\cos\theta_1 \tag{12}$$

Similarly, when the oil droplet advances from the position A to C (see Figure 5), the respectively geometrical relationship parameter and the relative FEB can be obtained.

DOI: 10.1021/acsami.5b03533
ACS Appl. Mater. Interfaces 2015, 7, 10641−10649

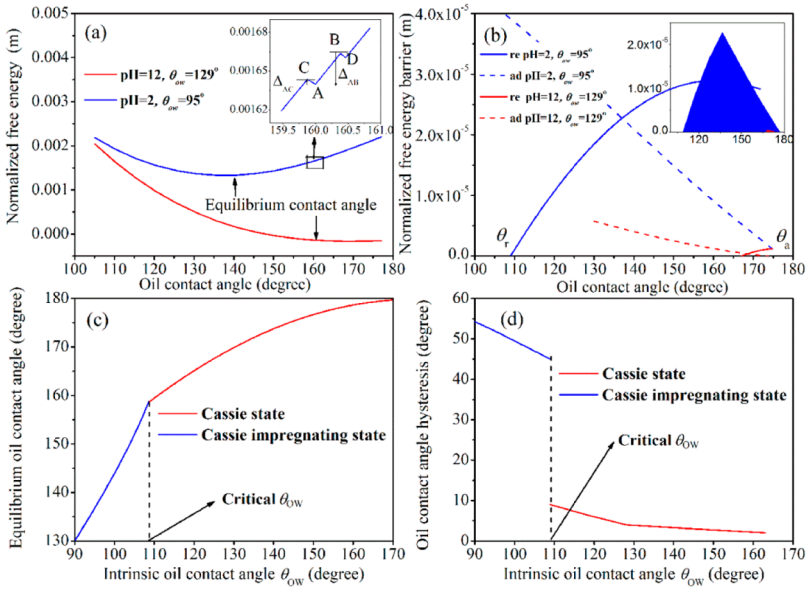

Figure 7. (a) Variation of normalized FE against apparent OCA for the Cassie impregnating state and the Cassie wetting state. The inset shows a larger view of a segment of the FE curve illustrating the FEB; positions A, B, and C correspond to those in Figure 4a. Δ_{AB} and Δ_{AC} stand for the FEB for receding and advancing contact line. (b) Variations of normalized advancing and receding free energy barrier (FEB) against apparent OCA for different intrinsic OCA with the Cassie impregnating and the Cassie state. (c) Dependent of EOCA with respect to intrinsic OCA with the Cassie impregnating and the Cassie wetting states. (d) Variations of OCAH versus the intrinsic OCA for systems. (L = 0.01 m, b_1 =50 μm, R_1 = 25 μm, b_2 = 0.5 μm, R_2 = 0.25 μm).

$$\theta_A\frac{{L_A}^2}{\sin^2\theta_A} - {L_A}^2\cot\theta_A + \frac{L_A}{b_1+2R_1}\left[(b_1+2R_1)R_1 - \frac{\pi{R_1}^2}{2}\right] = \theta_C\frac{{L_C}^2}{\sin{\theta_C}^2} - {L_C}^2\cot\theta_C - \frac{L_C}{b_1+2R_1}\left(\frac{\pi{R_1}^2}{2}\right) \quad (13)$$

$$\frac{\Delta F_{A\to C}}{\gamma^{ow}} = \theta_C\frac{L_C}{\sin\theta_C} - \theta_A\frac{L_A}{\sin\theta_A} - \left(\frac{\pi R_1}{2}\right)\cos\theta_1 \quad (14)$$

3.2.2. Gibbs FE and FEB Analysis for the Oil Cassie State. For a microtexture composite state, as the oil droplet edge changes from one semicircular protrusion to the nearby one, there also exist one metastable and one unstable state. The line B_1B_2 defines the internal oil−water interface in a microtexture composite case (see Figure 6). When the oil droplet recedes from position A to B_1, the droplet edge follows the solid surface under out energy. Further when point B_1 arrives, the droplet does not follow the solid surface and jumps from B_1 to B_2. Then it follows the solid surface to arrive at the equilibrium position with point D. When the oil droplet edge recedes from point B_2 to D, the force vector leads to movement of the oil droplet edge farther from point B_2. Thus, the position of point B_2 is the unstable state which possesses the local maximum free energy during the movement. While the oil droplet edge advances from position A to C, the movement of the droplet edge approaching point A can be caused by the force vector. Thus, point A is another unstable state which has the local maximum free energy when the edge of the droplet is advancing from one semicircular microtexture metastable position to the next. Similarly, the relationship geometrical parameter and the FEB for transition, respectively, can be written as

$$\theta_A\frac{{L_A}^2}{\sin^2\theta_A} - {L_A}^2\cot\theta_A + \frac{L_A}{b_1+2R_1}[(b_1+2R_1)(R_1-R_1\cos\alpha) - {R_1}^2(\alpha_1-\sin\alpha_1\cos\alpha_1)] = \theta_B\frac{{L_B}^2}{\sin{\theta_B}^2} - {L_B}^2\cot\theta_B - \frac{L_B}{b_1+2R_1}{R_1}^2(\alpha_1-\sin\alpha_1\cos\alpha_1) \quad (15)$$

$$\frac{\Delta F_{A\to B}}{\gamma^{ow}} = \theta_B\frac{L_B}{\sin\theta_B} - \theta_A\frac{L_A}{\sin\theta_A} + R_1\alpha_1\cos\theta_1 - (D-D_1) \quad (16)$$

$$\theta_A\frac{{L_A}^2}{\sin^2\theta_A} - {L_A}^2\cot\theta_A + \frac{L_A}{b_1+2R_1}[(b_1+2R_1)(R_1-R_1\cos\alpha_1) - {R_1}^2(\alpha_1-\sin\alpha_1\cos\alpha_1)] = \theta_C\frac{{L_C}^2}{\sin{\theta_C}^2} - {L_C}^2\cot\theta_C - \frac{L_C}{b_1+2R_1}{R_1}^2(\alpha_1-\sin\alpha_1\cos\alpha_1) \quad (17)$$

$$\frac{\Delta F_{A\to C}}{\gamma^{ow}} = \theta_C\frac{L_C}{\sin\theta_C} - \theta_A\frac{L_A}{\sin\theta_A} - R_1\alpha_1\cos\theta_1 \quad (18)$$

Combining eqs 7−18, the FE and FEB curve with the Cassie impregnating and Cassie wetting state are obtained.

3.2.3. Discussion. In this section, various CA and CAH from the calculations of FE and FEB curves are shown in Figure 7a. It is clear that one value of the lowest FE associated with equilibrium oil CA (EOCA) can be found. From the inset of Figure 7a, one can see that, if OCA varies slightly on the value of 10^{-2} degree, a fluctuation can be seen in local FE curve. This means that there is multivalued local minimum FE and maximum FE, corresponding to metastable and unstable equilibrium states. Furthermore, based on the same geometrical value with different intrinsic OCA as illustrated in Figure 7a,

DOI: 10.1021/acsami.5b03533
ACS Appl. Mater. Interfaces 2015, 7, 10641−10649

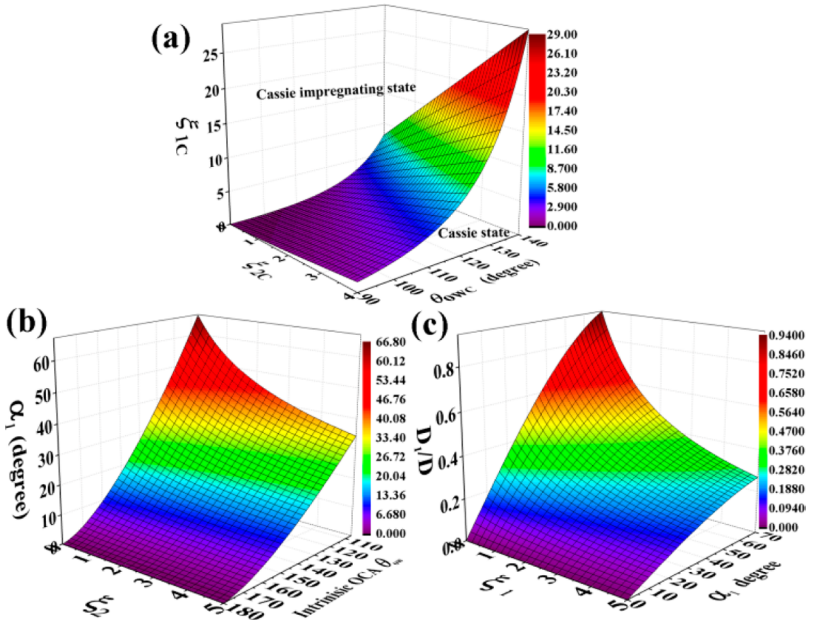

Figure 8. (a) The relationship for the transition between Cassie impregnating state and Cassie state versus the critical oil intrinsic CA and the micro- and nanotexture ratio of semicircular base distance and radius. (b) Variations of effective slope α_1 with microtexture for Cassie wetting state versus the oil intrinsic CA and the nanotexture ratio of semicircular base distance and radius. (c) Oil−water contact area under the oil droplet parameter D_1/D with the semicircular microtexture ratio of semicircular base distance and radius and slope for the Cassie wetting state.

the advancing and receding FEB for the Cassie impregnating and Cassie wetting state are shown in Figure 7b. The advances (θ_a), recessions CA (θ_r) and CAH defined as ($\theta_a - \theta_r$) are produced by the intersecting values of advancing and receding FE curves with the *x*-axis, respectively. Importantly, it is noted that the CAH under an ideal situation is different from the experimental results. In fact, the wetting transition behavior is dramatically influenced by outer vibration energy. When FEB between the Cassie impregnating state and the Cassie state can be overtaken by outer vibration energy, an oil droplet will transfer from the Cassie impregnating state to the Cassie state. Considering external vibrational energy, the CAH index can be defined.[41] The area of the shaded region which can be surrounded by the advancing FEB curve, receding FEB curve, and *x*-axis stands for the CAH index. From the inset of Figure 7b, one can see that the shaded region for the acid solution (pH = 2) is much larger than that of the basic (pH = 12) solution, indicating that the oil droplet adhesive force with the acid solution is much bigger than that with the basic solution. The result is consistent with experimental results.

In underwater three phase systems, the carboxylic acid groups are protonated or deprotonated by the acidic or basic solution, resulting in the variation of intrinsic OCA on responsive copper mesh films, while surface chemistry (intrinsic OCA) is vital to determining the value of the oil contact angle (OCA) and OCAH. Therefore, in this system, the controllable oil adhesion is caused by the different oil wetting states on the responsive superoleophobic surface that results from the difference of intrinsic OCA under different environmental pH value. The results were produced by the theory of thermodynamic analysis. The thermodynamic analysis result is consistent with the reference results under similar environmental conditions.[28,33,42] Thus, the oil wetting behavior can be manipulated by changing the pH value of the solution. For application of oleophobic materials, the underwater−oil intrinsic contact angle (OCA) larger than 90° is investigated. Herein, the interfacial oil adhesion behavior for superoleophobic surfaces is mainly investigated. The oil adhesion can be analyzed by the oil contact angle hysteresis (OCAH). Based on the FE and FEB curves, when the vibrational energy is equal to zero, variations of EOCA and OCAH against oil intrinsic contact angle for systems are shown in Figure 7c and d. One can note that there is a critical intrinsic OCA $\theta_{ow} = 109° \pm 1°$; when θ_{ow} is larger than the critical value, the system will stay in the Cassie wetting state; on the contrary, when θ_{ow} is lower than the critical value, the system will stay in the Cassie impregnating state. For the fixed geometrical parameter, substituting the critical intrinsic OCA value into eq 7, one can obtain $\theta_1 = 136.8° \pm 2°$, which is the effectively critical intrinsic OCA where the nanosemicircular structure is downsized. The results imply that the critical intrinsic OCA and OCAH can be diminished by the existence of nanosemicircular structure. Thus, the scope to achieve superoleophobic material has been expanded by the existence of nanosemicircular structure. Furthermore, It can be seen that the EOCA increases dramatically with the increasing in intrinsic OCA for the Cassie impregnating state, indicating that the superoleophobic has been enhanced with increasing intrinsic OCA of an oil droplet in water, especially for the Cassie impregnating state. Meanwhile, it should be also noted that for fixed semicircular base radius and distance, the oil contact angle hysteresis (OCAH) always decreases with increasing intrinsic OCA as the free energy barrier equals zero, whereas the OCAHs with the Cassie impregnating wetting state are relatively larger than that of the Cassie wetting state, reflecting that for fixed semicircular base radius and distance, the underwater−oil adhesion force can be minimized for self-cleaning properties in the Cassie wetting state. Therefore, the size of oil adhesive force depends on the oil wetting state.

Combining eqs 5−8, the critical condition between the Cassie impregnating state and Cassie states is obtained if both

DOI: 10.1021/acsami.5b03533
ACS Appl. Mater. Interfaces 2015, 7, 10641−10649

EOCA of the Cassie impregnating state and Cassie state are equal. Thus, the condition of the transition can be written as

$$\xi_{1C} = \frac{(\pi - 2\theta_{1C})\cos\theta_{1C} + 2(\sin\theta_{1C} - 1)}{1 + \cos\theta_{1C}} \quad (19)$$

$$\theta_{1C} = \mathrm{Arccos}\left(\frac{2(\pi - \theta_{owc})}{2 + \xi_{2C}}\cos\theta_{owc} + \frac{2\sin(\pi - \theta_{owc})}{2 + \xi_{2C}} - 1\right) \quad (20)$$

where $\xi_{1C} = b_1/R_1$ and $\xi_{2C} = b_2/R_2$ is the critical ratio of the base distance and radius with semicircular micro- and nanotexture; θ_{lC} and θ_{OWC} stand for the critical value of the effective angle θ_l and intrinsic OCA θ_{OW}. The intrinsic OCA and micro- and nanotexture semicircular and geometrical parameter affect the possibility of the transition between the Cassie impregnating state and Cassie states as shown in Figure 8a. It is obvious that the oil wetting state is closely related to the intrinsic OCA and micro- and nanotexture geometrical parameter. For the fixed nanotexture geometrical parameters and the intrinsic OCA, the wetting state may be transferred from the Cassie state to Cassie impregnating state with increasing the ratio of microtextures of semicircular, while the situation is opposite that of the nanotextures, one can see that for fixed the microtexture geometrical parameters and the intrinsic OCA, the wetting state may be transferred from the Cassie impregnating state to the Cassie state with increasing the ratio of semicircular nanotextures. The oil droplet adhesion will be enhanced with increasing the solid−oil contact area. For the Cassie impregnating state, the nanosemicircular slope α_2 decreases with increasing the intrinsic OCA, indicating that the oil adhesive force will be decreased with increasing intrinsic OCA. Meanwhile, from the conclusion and the expression of roughness r_1, one can also find that the oil contact area which can measured the oil adhesive force decreases with increasing the micro- and nanosemicircular ratio ξ_1 or ξ_2 for the Cassie impregnating state. Furthermore, the main parameter of effective microtexture slope angle α_1 is dramatically influenced by intrinsic OCA and the nanotexture geometrical parameter as shown in Figure 8b, one can see that the intrinsic OCA and nanotexture ratio geometrical parameter (ξ_2) have an equally effect on the changing of value α_1, that is, at a given parameter with the microtexture geometrical parameter, the adhesion force will be decreased by increasing the geometrical nanotexture ratio (ξ_2) or the intrinsic OCA. Here, we define the ratio value of D_1/D as shown in Figure 6. Importantly investigation shows that the solid and oil contact area is eliminated with decreasing in the ratio D_1/D value, leading to the surface oil adhesion and OCAH decrease. It is interesting to note that the ratio value D_1/D decreases with increasing the ratio of the microtexture (ξ_1) or decreasing in the angle α_1, as illustrated in Figure 8c. Therefore, the above results demonstrate that the trend which the parameters ξ_1, ξ_2, and θ_{OW} affect the oil adhesive force keeps unchanged in the wetting system, while the oil adhesive force depends on the wetting state.

4. CONCLUSION

In this article, pH-controllable underwater−oil adhesion and superoleophobic wetting behavior on the hierarchical-structured copper mesh films were investigated. Based on the thermodynamic analysis, a reasonable mechanism of the pH-controllable underwater−oil adhesion and superoleophobic wetting behavior observed on the surface has been revealed in an underwater three-phase system. In theory, the oil Cassie impregnating and Cassie wetting state on a more general micro- and nanoscale hierarchical semicircular structure has been proposed. Furthermore, the variation of chemistry (intrinsic oil contact angle (OCA)) parameters of the responsive semicircular microtexture that due to the carboxylic acid groups are protonated or deprotonated by the acidic solution or basic solution on FE with its barrier and EOCA and oil contact angle hysteresis (OCAH) are symmetrically discussed. It should be noted that the surface is underwater superoleophobic under different pH values of the solution; however, the underwater−oil adhesion on the surface is dramatically influenced by the pH value of solution. In underwater−water/oil/solid systems, the wetting mechanism reveals that the difference with underwater OCA and oil adhesion of the responsive copper mesh film under different pH values of solution are caused by the different oil wetting state that results from combining the changing intrinsic OCA and micro or nanostructures. These results are in good agreement with the experiment. The above results are hopeful to give some criteria for optimization design of practical superoleophobic surfaces and prediction of superoleophobic wetting behavior.

5. EXPERIMENTAL SECTION

Materials. Copper mesh films purchased from a local wire mesh store. *n*-Octadecylthiol (96%) was purchased from across organics. KOH, NaOH, and HCl were analytical-grade reagents. HCl and NaOH were used to regulate the acid−base property of the aqueous media.

Fabrication the Nanowire on the CMF. The original copper mesh films were immersed in diluted HCl (2 mol L^{-1}) to remove any surface oxide layer and sequentially cleaned with deionized water and acetone for at least three times. Then, the copper mesh films were dried by nitrogen gas for 5 min first. The $Cu(OH)_2$ nanowires were coated on the copper mesh film by a electrochemical deposition method. The copper mesh film was considered as the working electrode whereas the stainless steel sheet (surface area = 2 cm^2) was considered as the counter electrode. The reference electrode was a saturated calomel electrode. The $Cu(OH)_2$ nanowires was grown under a constant current density of 2 mA cm^{-2} in KOH (2 mol L^{-1}) aqueous solution for 2500 s at room temperature. Finally, the copper mesh film with $Cu(OH)_2$ was picked up from the solution, washed with distilled water, and dried in a N_2 stream.

Modification Responsive Molecules on the CMF. After $Cu(OH)_2$ nanowires were electrochemically deposited on the CMF, the CMF was coated with a layer of Au using a sputter coater. Then the copper meshes were dipped into a mixed thiol ethanol solution of $HS(CH_2)_9CH_3$ and $HS(CH_2)_{10}COOH$ for about 12 h. we keep the total concentration with 1 mmol L^{-1} and the concentration fraction of $HS(CH_2)_9CH_3$ and $HS(CH_2)_{10}COOH$ was set as 2:3. After the thiol modification, the CMFs were picked up and washed with anhydrous ethanol and dried in a drying oven.

Instrumentation and Characterization. Scanning electronmicroscopy images comes from JEOL JSM-5600LV scanning electron microscopes with Au-sputtered specimens. The water and oil contact angles were obtained by a DSA 100 instrumentation (kruss company, Germany). The acidic and basic aqueous solutions consist of HCl and NaOH. The pH values were measured by pH instrumentation (PB-10, Sartorius). The adhesive force was obtained by a high sensitivity microelectromechanical balance (Dataphysics DCAT 11, Germany).

AUTHOR INFORMATION

Corresponding Author

*E-mail: zguo@licp.cas.cn; Tel: 0086-931-4968105; Fax: 0086-931-8277088.

DOI: 10.1021/acsami.5b03533
ACS Appl. Mater. Interfaces 2015, 7, 10641−10649

Notes

The authors declare no competing financial interest.

■ ACKNOWLEDGMENTS

The China National Natural Science Foundation (Nos. 11172307, 21203217), the Western Light Talent project, and the Top Hundred Talents project of Chinese Academy of Sciences.

■ REFERENCES

(1) Guo, Z. G.; Liu, W. M. Biomimic from the superhydrophobic plant leaves in nature Binary structure and unitary structure. *Plant Sci.* **2007**, *172*, 1103−1112.
(2) Feng, L.; Zhang, Y. A.; Xi, J. M.; Zhu, Y.; Wang, N.; Xia, F.; Jiang, L. Petal Effect: A Superhydrophobic State with High Adhesive Force. *Langmuir* **2008**, *24*, 4114−4119.
(3) Liu, M. J.; Wang, S. T.; Wei, Z. X.; Song, Y. L.; Jiang, L. Bioinspired Design of a Superoleophobic and Low Adhesive Water/Solid Interface. *Adv. Mater.* **2009**, *21*, 665−669.
(4) Gao, X. F.; Jiang, L. Biophysics: Water-repellent legs of water striders. *Nature* **2004**, *432*, 36−36.
(5) Li, C.; Zhang, Y. Y.; Ju, J.; Cheng, F. T.; Liu, M. J.; Jiang, L.; Yu, Y. L. In Situ Fully Light-Driven Switching of Superhydrophobic Adhesion. *Adv. Funct. Mater.* **2012**, *22*, 760−763.
(6) Ng, C. C. A.; Magenau, A.; Ngalim, S. H.; Ciampi, S.; Chockalingham, M.; Harper, J. B.; Gaus, K.; Gooding, J. J. Using an Electrical Potential to Reversibly Switch Surfaces between Two States for Dynamically Controlling Cell Adhesion. *Angew. Chem., Int. Ed.* **2012**, *51*, 7706−7710.
(7) Hong, X.; Gao, X. F.; Jiang, L. Application of Superhydrophobic Surface with High Adhesive Force in No Lost Transport of Superparamagnetic Microdroplet. *J. Am. Chem. Soc.* **2007**, *129*, 1478−1479.
(8) Zarzar, L. D.; Kim, P.; Aizenberg, J. Bio-inspired Design of Submerged Hydrogel-Actuated Polymer Microstructures Operating in Response to pH. *Adv. Mater.* **2011**, *23*, 1442−1446.
(9) Wang, D. A.; Liu, Y.; Liu, X. J.; Zhou, F.; Liu, W. M.; Xue, Q. J. Towards a tunable and switchable water adhesion on a TiO_2nanotube film with patterned wettability. *Chem. Commun.* **2009**, *45*, 7018−7020.
(10) Geyer, F. L.; Ueda, E.; Liebel, U.; Grau, N.; Levkin, P. A. Superhydrophobic−Superhydrophilic Micropatterning: Towards Genome-on-a-Chip Cell Microarrays. *Angew. Chem., Int. Ed.* **2011**, *50*, 8424−8427.
(11) Zhao, B.; Moore, J. S.; Beebe, D. J. Surface-Directed Liquid Flow Inside Microchannels. *Science* **2001**, *291*, 1023−1026.
(12) Cheng, Z. J.; Du, M.; Fu, K. W.; Zhang, N. Q.; Sun, K. N. pH-Controllable Water Permeation through a Nanostructured Copper Mesh Film. *ACS Appl. Mater. Interfaces.* **2012**, *4*, 5826−5832.
(13) Cheng, Z. J.; Lai, H.; Du, Y.; Fu, K. W.; Hou, R.; Li, C.; Zhang, N. Q.; Sun, K. N. pH-Induced Reversible Wetting Transition between the Underwater Superoleophilicity and Superoleophobicity. *ACS Appl. Mater. Interfaces* **2014**, *6*, 636−641.
(14) Tian, D. L.; Zhang, X. F.; Zhai, J.; Jiang, L. Photocontrollable Water Permeation on the Micro/Nanoscale Hierarchical Structured ZnO Mesh Films. *Langmuir* **2011**, *27*, 4265−4270.
(15) Wang, B.; Liang, W. X.; Guo, Z. G.; Liu, W. M. Biomimetic super-lyophobic and super-lyophilic materials applied for oil/water separation: a new strategy beyond nature. *Chem. Soc. Rev.* **2015**, *44*, 336−361.
(16) Jiang, T.; Guo, Z. G.; Liu, W. M. Biomimetic superolephobic surfaces: focusing on their fabrication and applications. *J. Mater. Chem. A* **2015**, *3*, 1811−1827.
(17) Si, Y. F.; Guo, Z. G. Superhydrophobic nanocoatings: From materials to fabrications and to applications. *Nanoscale* **2015**, *7*, 5922−5946.
(18) Cheng, Z. J.; Lai, H.; Du, Y.; Fu, K. W.; Hou, R.; Zhang, N. Q.; Sun, K. N. Underwater Superoleophilic to Superoleophobic Wetting Control on the Nanostructured Copper Substrates. *ACS Appl. Mater. Interfaces.* **2013**, *5*, 11363−11370.
(19) Yong, J. L.; Chen, F.; Yang, Q.; Zhang, D. S.; Farooq, U.; Du, G. Q.; Hou, X. Bioinspired underwater superoleophobic surface with ultralow oil-adhesion achieved by femtosecond laser microfabrication. *J. Mater. Chem. A* **2014**, *2*, 8790−8795.
(20) Lai, Y. K.; Pan, F.; Xu, C.; Fuchs, H.; Chi, L. F. In Situ Surface-Modifi cation-Induced Superhydrophobic Patterns with Reversible Wettability and Adhesion. *Adv. Mater.* **2013**, *25*, 1682−1685.
(21) Cheng, Q. F.; Li, M. Z.; Yang, F.; Liu, M. J.; Li, L.; Wang, S. T.; Jiang, L. An underwater pH-responsive superoleophobic surface with reversibly switchable oil-adhesion. *Soft Matter* **2012**, *8*, 6740−6743.
(22) Quere, D. Wetting and roughness. *Annu. Rev. Mater. Res.* **2008**, *38*, 71−99.
(23) Extrand, C. W. Criteria for Ultralyophobic Surfaces. *Langmuir* **2004**, *20*, 5013−5018.
(24) Extrand, C. W. Model for Contact Angles and Hysteresis on Rough and Ultraphobic Surfaces. *Langmuir* **2002**, *18*, 7991−7999.
(25) Patankar, N. A. On the Modeling of Hydrophobic Contact Angles on Rough Surfaces. *Langmuir* **2003**, *19*, 1249−1253.
(26) Nosonovsky, M.; Bhushan, B. Roughness optimization for biomimetic superhydrophobic surfaces. *Microsyst. Technol.* **2005**, *11*, 535−549.
(27) Marmur, A. Underwater Superhydrophobicity: Theoretical Feasibility. *Langmuir* **2006**, *22*, 1400−1402.
(28) Marmur, A. Adhesion and Wetting in an Aqueous Environment: Theoretical Assessment of Sensitivity to the Solid Surface Energy. *Langmuir* **2004**, *20*, 1317−1320.
(29) Marmur, A. Superhydrophobic and superhygrophobic surfaces: from understanding non-wettability to design considerations. *Soft Matter* **2013**, *9*, 7900−7904.
(30) Li, W.; Amirfazli, A. A thermodynamic approach for determining the contact angle hysteresis for superhydrophobic surfaces. *J. Colloid Interface Sci.* **2005**, *292*, 195−201.
(31) Tie, L.; Guo, Z. G.; Li, W. Optimal design of superhydrophobic surfaces using a paraboloid Microtexture. *J. Colloid Interface Sci.* **2014**, *436*, 19−28.
(32) Li, W.; Fang, G. P.; Li, Y. F.; Qiao, G. J. Anisotropic Wetting Behavior Arising from Superhydrophobic Surfaces: Parallel Grooved Structure. *J. Phys. Chem. B* **2008**, *112*, 7234−7243.
(33) Bhushan, B.; Jung, Y. C. Wetting Behavior of Water and Oil Droplets in Three-Phase Interfaces for Hydrophobicity/philicity and Oleophobicity/philicity. *Langmuir* **2009**, *25* (24), 14165−14173.
(34) Youngblood, J. P.; McCarthy, T. J. Ultrahydrophobic Polymer Surfaces Prepared by Simultaneous Ablation of Polypropylene and Sputtering of Poly(tetrafluoroethylene) Using Radio Frequency Plasma. *Macromolecules* **1999**, *32*, 6800−6806.
(35) Cassie, A. B. D.; Baxter, S. Wettability of Porous Surfaces. *Trans. Faraday Soc.* **1944**, *40*, 546−551.
(36) Wenzel, R. Resistance of Solid Surfaces to Wetting by Water. *Ind. Eng. Chem.* **1936**, *28*, 988−994.
(37) Liu, T. Q.; Sun, W.; Sun, X. Y.; Ai, H. R. Thermodynamic Analysis of the Effect of the Hierarchical Architecture of a Superhydrophobic Surface on a Condensed Drop State. *Langmuir* **2010**, *26* (18), 14835−14841.
(38) Marmur, A. Wetting on Hydrophobic Rough Surfaces: To Be Heterogeneous or Not To Be? *Langmuir* **2003**, *19*, 8343−8348.
(39) Johnson, R. E.; Dettre, R. H. Contact Angle Hysteresis - II. Contact Angle Measurements on Rough Surfaces. *Adv. Chem. Ser.* **1964**, *43*, 112−135.
(40) Liu, M. J.; Xue, Z. X.; Liu, H.; Jiang, L. Surface Wetting in Liquid−Liquid−Solid Triphase Systems: Solid-Phase-Independent Transition at the Liquid−Liquid Interface by Lewis Acid− Base Interactions. *Angew. Chem., Int. Ed.* **2012**, *51*, 1−5.
(41) Lee, D. J.; Kim, H. M.; Song, Y. S.; Youn, J. R. Water Droplet Bouncing and Superhydrophobicity Induced by Multiscale Hierarchical Nanostructures. *ACS Nano* **2012**, *6* (9), 7656−7664.

DOI: 10.1021/acsami.5b03533
ACS Appl. Mater. Interfaces 2015, 7, 10641−10649

(42) Bhushan, B.; Her, E. K. Fabrication of Superhydrophobic Surfaces with High and Low Adhesion Inspired from Rose Petal. *Langmuir* **2010**, *26* (11), 8207−8217.

DOI: 10.1021/acsami.5b03533
ACS Appl. Mater. Interfaces 2015, 7, 10641−10649